Spontaneous Vesicle Formation in a Block Copolymer System

ARTICLE *in* THE JOURNAL OF PHYSICAL CHEMISTRY B · JUNE 2004

Impact Factor: 3.3 · DOI: 10.1021/jp031313u

5 AUTHORS, INCLUDING:

Karin Schillén
Lund University
80 PUBLICATIONS **2,871** CITATIONS
SEE PROFILE

Ulf Olsson
Lund University
269 PUBLICATIONS **7,028** CITATIONS
SEE PROFILE

Spontaneous Vesicle Formation in a Block Copolymer System

Karin Bryskhe,* Jörgen Jansson, Daniel Topgaard, Karin Schillén, and Ulf Olsson

Physical Chemistry 1, Center for Chemistry and Chemical Engineering, Lund University, P.O. Box 124, S-221 00 Lund, Sweden

Received: December 11, 2003

We have investigated the formation of vesicles in the binary system of a triblock copolymer of poly(ethylene oxide) (PEO) and poly(propylene oxide) (PPO) with the average composition $EO_5PO_{68}EO_5$ in water. Vesicles are formed when a solution of unimers is heated into a two-phase region where, at equilibrium, a concentrated lamellar phase coexists with a dilute solution of unimers. The vesicles were characterized by cryo-TEM, static and dynamic light scattering, and NMR experiments. The average vesicle radius is approximately 60 nm, with an exponential size distribution, and the concentration of vesicles depends strongly on the temperature. The vesicles remain stationary on the time scale of hours. A striking observation is that, on this time scale, both the vesicle size distribution and the concentration of vesicles are reversible with respect to temperature cycles. However, on the time scale of weeks a sedimentation is observed in the solutions.

1. Introduction

One class of water-soluble block copolymers, are the triblock copolymers of poly(ethylene oxide) (PEO) and poly(propylene oxide) (PPO), often abbreviated as PEO−PPO−PEO or $EO_nPO_mEO_n$.[1−3] The $EO_nPO_mEO_n$ polymers, also called Pluronics, have been investigated for pharmaceutical use and as a component in different drug delivery systems.[4−6] At present, the U.S. FDA has approved a number of Pluronics to be used in formulations for humans, but not the one used in this study. These copolymers exist in a wide range of different compositions and display a rich phase behavior in water, depending on their relative block lengths.[7,8] It is well established that the more hydrophilic copolymers with a high PEO/PPO ratio associate into micelles composed of a PPO-rich core and a PEO-rich corona with a spherical or rodlike shape, depending on temperature.[9−12] Recently, we have also reported that unilamellar vesicles can be formed in water by a particular copolymer with the average composition $EO_5PO_{68}EO_5$, denoted L121.[13]

Vesicle structures are well-known from investigations of lipids and surfactants and are composed of a bilayer shell enclosing a pool of solvent.[14−16] They are generally considered to be metastable structures where thermodynamic equilibrium corresponds to a lamellar phase, possibly coexisting with excess solvent. However, there are also several reports in the literature claiming that thermodynamically stable vesicles have been found.[17−20] The problem of thermodynamic equilibrium can be a difficult issue to reveal experimentally. The coarsening mechanism of Ostwald ripening is expected to be very slow in vesicle systems and may even lead to a kinetically trapped size distribution.[21]

There are some reports in the literature on vesicle formation of diblock and multiblock copolymers in dilute solutions of selective solvents.[22−29] Vesicles of polystyrene−poly(acrylic acid) (PS−PAA) and PS−PEO diblock copolymers were prepared in aqueous solutions using a dialysis method.[30,31] For these vesicles, the water-insoluble PS block is in a glassy state at ambient temperatures, making the vesicles kinetically trapped. A study on a polybutadiene−PAA (PBD−PAA) copolymer/water system has concluded that the vesicular morphology is not controlled by the glass transition temperature of the nonsoluble block.[32] Finally, other publications have reported on the formation of multilamellar block copolymer vesicles ("onions") in concentrated systems.[33−37]

In a recent publication, we reported that vesicles can be formed in dilute aqueous solutions of the bilayer forming PEO−PPO−PEO block copolymer L121.[13] Those samples were prepared by extrusion of a dilute dispersion of the concentrated lamellar phase several times through a porous membrane. In the phase diagram of the L121/D_2O system, that is shown in Figure 1 (redrawn from ref 38), this two-phase region is present at room temperature. As can be noticed, and in common with other PEO−PPO−PEO/water systems, the self-assembly behavior is strongly temperature-dependent, and at lower temperatures a homogeneous isotropic solution phase is found in the L121/water system. The boundaries of the different one-phase regions are indicated with solid lines; in Figure 1 the broken lines are estimated three-phase lines when assuming L121 to be a pure single component.

In the present study, we have continued to investigate vesicle formation in this system. Here, we have let a dilute solution originally in the L_1 phase be simply heated across the phase boundary into the $L_1 + L_\alpha$ coexistence region without agitation or extrusion. The vesicles formed have been characterized by cryo transmission electron microscopy (cryo-TEM), static and dynamic light scattering (SLS, DLS), and NMR self-diffusion and chemical shift experiments. The paper is structured as follows. First, we present the experimental procedures and the experimental techniques used. Then we present and discuss the results from the different experiments, and finally, we end with a short summary and conclusions.

2. Experimental Section

Materials and Sample Preparation. The poly(ethylene oxide)−poly(propylene oxide)−poly(ethylene oxide) (PEO−

* Corresponding author. E-mail: Karin.Bryskhe@fkem1.lu.se.

10.1021/jp031313u CCC: $27.50
Published on Web 06/22/2004

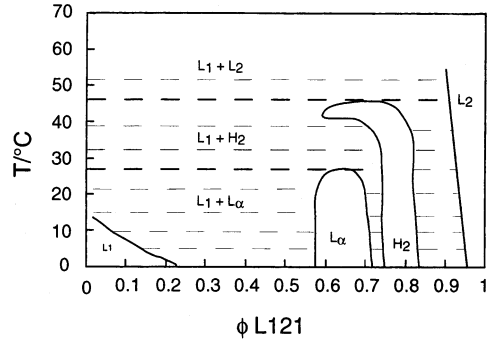

Figure 1. Phase diagram of the $EO_5PO_{68}EO_5/D_2O$ system. The boundaries of the various one-phase regions are indicated with solid lines, the two-phase areas are indicated with broken lines, and the three-phase lines are marked with bold broken lines. L_1, L_α, H_2, and L_2 correspond to isotropic polymer solution, lamellar phase, reversed hexagonal phase, and concentrated polymer solution, respectively.

PPO−PEO) triblock copolymer L121 was obtained as a gift from BASF Corp., Mount Olive, NJ. The nominal molar mass of this copolymer is 4400 g mol^{-1}, and it has a density of 1.03 g/mL and a PPO content of 90 wt %; thus, the molecule can be represented as $EO_5PO_{68}EO_5$. Heavy water, D_2O, (99.80 at. % ^2H) was purchased from Dr. Glaser AG, Basel, Switzerland. All these chemicals were used without further purification. Ordinary water, H_2O, was treated with a Millipore-Q water purification system.

The L121 aqueous solutions were prepared individually by weighing the desired amounts of the components into glass tubes at room temperature. They were stored at 8 °C, corresponding to the L_1 phase, and then equilibrated for at least 20 min at the desired temperature before any experiments were carried out. These PEO−PPO−PEO copolymers are commercial materials having both composition (i.e., EO/PO ratio) and molecular weight polydispersity, and the mixture may contain a distribution of molecules having different amphiphilicity and self-assembly behavior.[9,39−44]

Cryo-TEM. Specimens for transmission electron microscopy were prepared in a controlled environment vitrification system (CEVS)[45] to avoid water evaporation and to ensure a fixed temperature (25 °C) of the solution during sample preparation. They were prepared as thin liquid films less than 100 nm thick on a lacey carbon filmed copper grid and quenched into liquid ethane. The technique, which has been described in detail by Bellare et al.,[45] leads to vitrified specimens, so that component segmentation, rearrangement, and water crystallization are prevented and the original microstructure is preserved during thermal fixation. The vitrified samples were stored under liquid nitrogen and transferred to the electron microscope (Philips CM120 BioTWIN Cryo) equipped with a postcolumn energy filter (GIF), using an Oxford CT3500 cryoholder and its workstation. The electron acceleration voltage was 120 kV, and the defocus was less than 1 μm. Images were collected under low dose conditions and recorded digitally with a CCD camera (Gatan MSC791). Before sample preparation in the CEVS, the samples were equilibrated at 25 °C for 3 or 18 h, respectively. Images taken after different equilibration times showed no significant differences.

Dynamic and Static Light Scattering. The experimental setup, which is described in detail in ref 42, is a laser light scattering ALV/DLS/SLS-5000F CGS-8F based compact goniometer system from ALV Gmbh, Langen, Germany, for simultaneous angular-dependent determination of dynamic light scattering (DLS) and static light scattering (SLS) including a solid-state, diode-pumped Nd:YAG laser from Coherent operating at 532 nm and at a constant output power of 400 mW, which is variable with an external attenuator from Newport Corp., USA. For DLS measurements using photon correlation spectroscopy, two multiple delay time digital correlators (ALV-5000/E and ALV-5000/FAST) with a total of 320 exponentially spaced channels were employed to construct the normalized time-correlation function of the scattered intensity, $g^{(2)}(t)$ (both pseudo-cross and auto-correlation were carried out). The intensity correlation functions are here presented as $g^{(2)}(t) - 1 = f(t)$, where t is the lag time in ms. $g^{(2)}(t)$ is in turn related to the normalized time correlation function of the electric field by Siegert's relation: $g^{(2)}(t) - 1 = \beta|g^{(1)}(t)|^2$, and on which light scattering models are based.

The SLS measurements were performed on the copolymer aqueous solutions (0.0025−0.05 wt %) without subtraction of the scattering from water and using toluene as standard. The refractive index increment, dn/dc, at 532 nm was determined using a DR-1 differential refractometer from ALV, which is incorporated in the overall DLS/SLS setup with an optical fiber. For the L121/water system studied here, dn/dc = 0.1309 ± 0.0006 mL/g at 8 °C, as measured on solutions with the concentration ranging from 1.25 to 10 wt %. The measured value of dn/dc was recalculated with respect to the L121 volume fraction, ϕ, yielding dn/dϕ = 0.135. For both the DLS and SLS measurements, the copolymer solutions were filtered cold (in the L_1 phase) through 0.20 μm Minisart filters from Sartorius directly into cylindrical scattering cells of borosilicate glass that were immersed into a thermostated container (VAT) containing toluene as the refractive index-matching liquid. The temperature was controlled to within ± 0.03 °C. Prior to the measurements, the copolymer solutions were equilibrated at the given temperature for at least 15 min.

To investigate the possibility of multiple scattering, additional transmittance (T) measurements were performed on a Perkin-Elmer Lambda 14 UV−Vis double-beam spectrophotometer at the same wavelength of 532 nm. The spectrophotometer contains a thermostated sample cell holder. The temperature was controlled by a Haake circulating water bath, which kept the temperature constant within ±0.1 °C. The transmittance was measured at 25 °C in 1 cm quartz cells.

Nuclear Magnetic Resonance. NMR self-diffusion experiments were performed on a Bruker DMX 200 spectrometer operating at a ^1H resonance frequency of 200.13 MHz. The instrument was equipped with a Bruker DIFF-25 gradient probe driven by a Bruker BAFPA-40 unit. Here, the temperature can be varied and controlled to an accuracy of ±0.2 °C. The self-diffusion experiments were performed using the stimulated echo technique, 90°−τ_1−90°−τ_2−90°−τ_1−signal detection, with one pulsed field gradient of strength g and duration δ in each τ_1-period.[46] The time between the leading edges of the gradient pulses is $\Delta = \tau_1 + \tau_2$. g was varied in 32 equal increments to the maximum value g_{max}. Because of the large difference in diffusion coefficient between unimer and vesicle, separate experiments were performed at 25 °C (0.01 wt %). The parameters were δ = 1 ms, Δ = 22.1 ms, and g_{max} = 9.63 T/m and δ = 2 ms, Δ = 53.2 ms, and g_{max} = 9.63 T/m, respectively. An additional experiment where the diffusion time was varied was performed at a higher L121 concentration (0.05 wt %). Due to the low copolymer concentrations used here, an extensive signal averaging was necessary in order to obtain an acceptable signal-to-noise ratio. In the extreme case, a diffusion experiment lasted for 60 h.

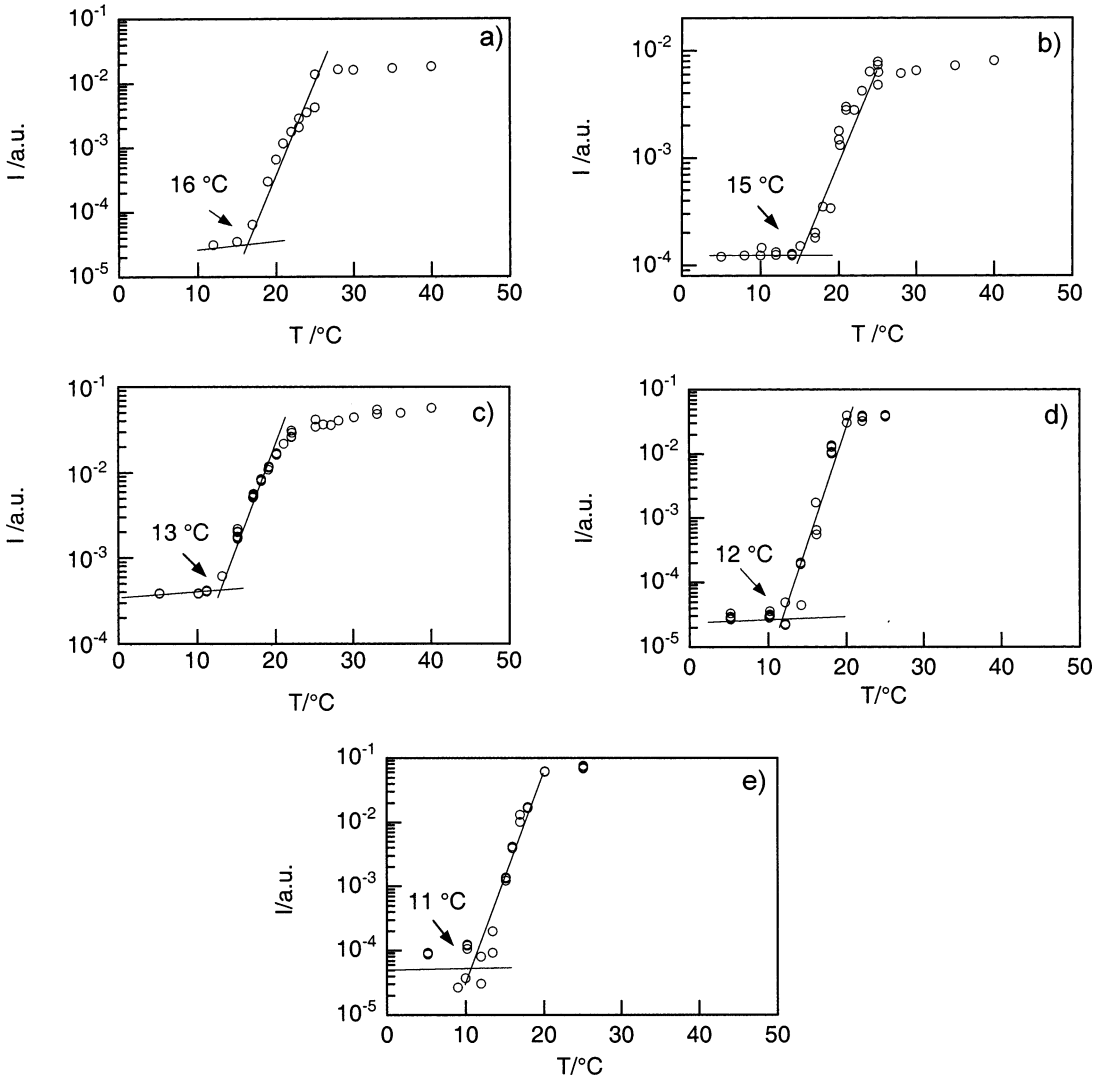

Figure 2. The scattered intensity (I) as a function of temperature (T) for different concentration of L121 (a) 0.0025 wt %, (b) 0.005 wt %, (c) 0.01 wt %, (d) 0.02 wt %, and (e) 0.05 wt %. The temperature for the sharp increase in intensity that is observed is indicated, and from these temperatures the phase diagram in Figure 3 was determined.

In the case of free (Gaussian) diffusion the attenuation of the signal intensities in the NMR diffusion experiment is given by[46]

$$E = \exp(-kD) \tag{1}$$

where

$$k \equiv \gamma^2 g^2 \delta^2 (\Delta - \delta/3) \tag{2}$$

Here, γ is the magnetogyric ratio ($\gamma = 2.67520 \times 10^8$ rad T^{-1} s^{-1} for protons). In the case when there exist several diffusion "sites" characterized by different diffusion coefficients (for example unimers and aggregates), a single-exponential echo decay indicates fast exchange between the different sites on the observation time scale, Δ, and only an average diffusion coefficient can be detected. In the case of slow exchange, on the other hand, the echo decay is given by sum of exponentials, each describing a given diffusion site.

^{1}H NMR spectra were also recorded on a Bruker DMX 500 spectrometer operating at a ^{1}H resonance frequency of 500 MHz with a resolution of 0.25 Hz. The pulse width used was 6 μs. The sample temperature was varied and controlled to an accuracy of $\pm$0.5 °C.

3. Results and Discussion

The L_1 Phase Boundary in the Dilute Regime. In very dilute copolymer solutions, the phase boundary of the L_1 phase is difficult to detect by the eye, and therefore the photomultiplier of the light scattering equipment was used instead. A dilute solution at low temperatures in the L_1 phase scatters very little light. However, when increasing the temperature, the scattered intensity increases rapidly with increasing temperature after passing a particular temperature, indicating the formation of large aggregates. The situation is illustrated in Figure 2a−e where we present total scattered intensity, normalized by the incoming laser intensity, recorded at the scattering angle $\theta = 90°$, as a function of the temperature for 5 different compositions between 0.0025 and 0.05 wt %. The onset of formation of large aggregates, we identify as the phase boundary of the L_1 phase, with higher temperatures corresponding to a two-phase equilibrium $L_1 + L_\alpha$. Hence, from the data in Figure 2a−e we have drawn a partial phase diagram shown in Figure 3 for these dilute conditions.

Only Unimers in the L_1-Phase. In the L_1 phase, the scattered intensity is essentially independent of the temperature. A NMR self-diffusion experiment performed at 10 °C (see Figure 8) for a sample of 0.01 wt % of L121 in D_2O, gave a copolymer (unimer) self-diffusion coefficient of $D = 6.6 \times 10^{-11}$ m^2/s^{-1}.

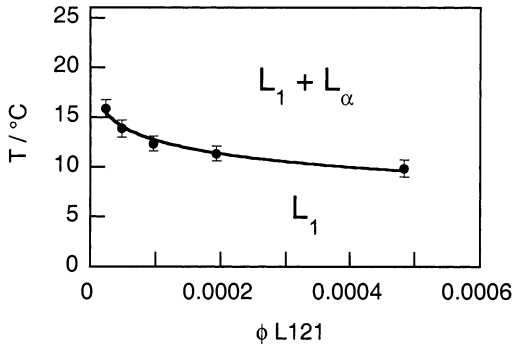

Figure 3. Phase diagram of the $EO_5PO_{68}EO_5/D_2O$ system at low concentrations of the polymer. The phase boundary between the L_1 phase and the two-phase region of L_1 and L_α is indicated with a solid line. Also, here L_1 and L_α correspond to isotropic polymer solution and lamellar phase.

Due to the low concentration, we have approximately $D \approx D_0$, where D_0 denotes the self-diffusion coefficient at infinite dilution, and we can thus directly calculate a hydrodynamic radius, R_H, according to the Stokes−Einstein relation

$$R_H = \frac{k_B T}{6\pi\eta_0 D_0} \tag{3}$$

Here, k_B is the Boltzmann constant, T is the absolute temperature, and η_0 is the viscosity of the solvent. The observed diffusion coefficient corresponds to $R_H = 1.9$ nm. This value is in very good agreement with the value 1.9 nm (*z*-average) previously determined at the same temperature and concentration, although in H_2O, using dynamic light scattering.[13] The large diffusion coefficient (i.e., small R_H) together with the temperature independence of the scattered intensity is a strong indication that the copolymer is present only as unimers in the L_1 phase at these concentrations. It is well established that a minor fraction of large particles containing a hydrophobic impurity can be detected below the critical aggregation temperature in these copolymer systems. This was also the case for the present L121 system.[13] However, the scattering intensity is still very low since they are small in number. When approaching bilayer formation at higher temperatures, we would expect micelles, if present, to increase in size with increasing temperature, since they become rodlike in some PEO−PPO−PEO systems[12] as commonly observed with nonionic surfactants of the ethylene oxide type.[47,48] Here, however, micelle formation does not seem to occur, and we can identify the phase boundary of the L_1 phase as a line of a critical aggregation (bilayer formation) concentration (or temperature), but where the large aggregates do not form a stable dispersion but aggregate in turn to eventually form a concentrated phase, the L_α phase. This transition has also been observed in a recent calorimetry study of the same copolymer.[49]

Unilamellar Vesicles in the $L_1 + L_\alpha$ Region. The aggregates formed when heating a dilute sample from the L_1 phase into the $L_1 + L_\alpha$ region are unilamellar vesicles. This can be seen in Figure 4, where we present a representative cryo-TEM image for a concentration of 0.01 wt %, vitrified from 25 °C. The image shows unilamellar vesicles of different radii in the range 30−200 nm. It is representative for how the size of the vesicles varies, where the number of relatively small vesicles will dominate over the number of larger vesicles. An additional observation is that the largest vesicle in Figure 4 is placed close to the supporting grid, where the concave film is thickest, i.e., also a size segregation takes place within the film. The largest vesicle shows also a darker centrum, which is an indication that the diameter is actually larger than the film thickness and therefore extends the surface of the film.

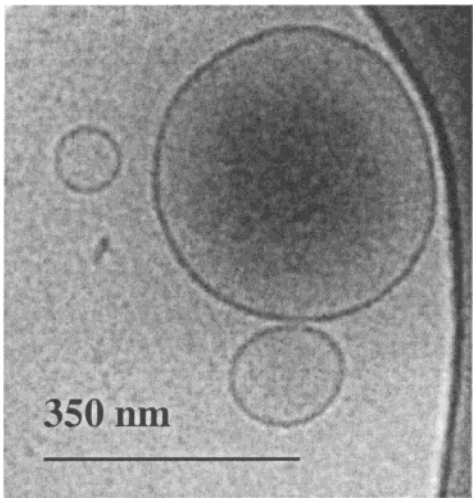

Figure 4. Representative Cryo-TEM image at 25 °C of the vesicles at 0.01 wt % of copolymer.

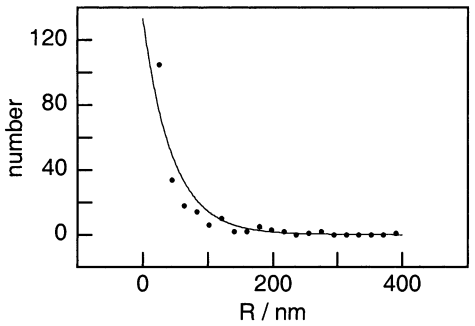

Figure 5. (●) represents the number distribution of the vesicle size obtained from the cryo-TEM images (0.01 wt %). (−) represents the distribution described by eq 4.

The vesicle size distribution was estimated for 0.01 wt % and 25 °C by analyzing a population of a total 205 number of vesicles. The number-average radius was calculated from the 205 vesicles analyzed, and a value of 58 nm was obtained. The results are presented in Figure 5 as a histogram. The size distribution can be approximated by an exponential

$$N(R) = N_{tot}\frac{\exp\{-R/\langle R\rangle\}}{\langle R\rangle} \tag{4}$$

where $N(R)$ is the number density of vesicles having a radius between R and $R + dR$, and $\langle R\rangle$ is the number-average radius. N_{tot} is the total number of vesicles per unit volume. Also in Figure 5 the exponential which gives the number-average radius of 58 nm is shown as a solid line, and as can be seen it describes the histogram well.

Vesicle Stability. When the fusion of vesicles is rare, vesicle dispersions often show a long time stability because coarsening through a ripening mechanism can be very slow and may even trap the system in a metastable size distribution.[21] In the present system, the vesicle dispersions appeared to be stable for many hours. There is also an additional explanation to this stability. For a 0.01 wt % solution at 25 °C the scattered intensity at $\theta = 90°$ was followed as a function of time over a period of 6.5 h, and the results are shown in Figure 6. As can be seen, there is essentially no variation of the scattered intensity, indicating that

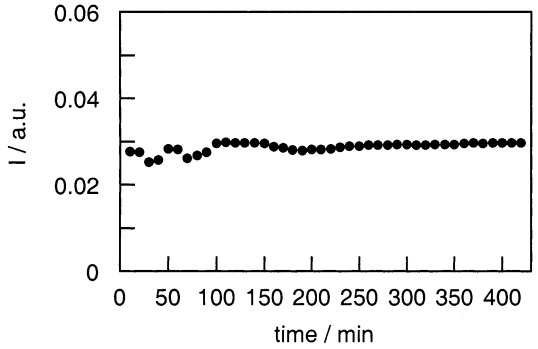

Figure 6. Scattered intensity (I) as a function of time (t) for a 0.01 wt % copolymer sample. The unchanged behavior of the intensity with time indicates that the aggregates are unchanged under the time period studied.

the vesicle size distribution is essentially stationary over this time period. In the cryo-TEM experiments we also compared images from samples with 3 h and 18 h equilibration times, respectively, and observed no differences between the two equilibration times. On the time scale of weeks, on the other hand, a sedimentation was observed in the samples. The sediments were not investigated in detail but may involve an aggregation of vesicles and eventually the formation of the lamellar phase.

The Vesicle Size Distribution. The size distribution of vesicles can also be estimated from SLS or DLS experiments. Because of the large vesicle size, the full form factor of the vesicles has to be taken into account:[50]

$$P(q,R) = \left(\frac{3}{u^3 - v^3}\right)^2 \left(u^3 \frac{j_1(qu)}{qu} - v^3 \frac{j_1(qv)}{qv}\right)^2 \qquad (5)$$

where $u = R + d/2$ and $v = R - d/2$. R is defined as the radius corresponding to the center of the vesicle wall, d is the vesicle wall thickness, $j_1(x)$ is the first-order spherical Bessel function, and q is the magnitude of the scattering vector. The vesicles are uncharged and very dilute, so we can neglect interactions and the structure factor is ≈ 1. In this case the normalized correlation function of the scattered electric field decays as a weighted sum of exponentials

$$g^{(1)}(t) = \frac{\int N(R)R^4 P(q,R) \exp\{-D(R)q^2 t\}\, dR}{\int N(R)R^4 P(q,R)\, dR} \qquad (6)$$

where the different vesicle sizes are weighted with respect to their relative concentration, $N(R)$, (i.e. the number-average size distribution) and their relative scattering power, $R^4P(q,R)$. $D(R)$ is the diffusion coefficient of a vesicle of radius R, and assuming $R = R_H$, we can use the Stokes−Einstein equation to relate $D(R)$ to the vesicles radius. Assuming the number-average size distribution, $N(R)$ to be exponential, we have use eqs 3, 4, and 6 in the expression $g^{(2)}(t) - 1 = \beta|g^1(t)|^2$ to fit the measured intensity correlation functions obtained at different q-values, i.e., different scattering angles, for the concentration 0.01 wt % at 25 °C, with $\langle R \rangle$ being the single fitting parameter. The results and corresponding fits are presented in Figure 7a−e. For lower q-values ($q < 8.14\ \mu m^{-1}$; $\theta = 30°$) the combination of eqs 3−6 describes the experimental data well. For example, the number-averaged radius $\langle R \rangle = 54$ nm obtained at $q = 5.19\ \mu m^{-1}$ ($\theta = 19°$) is in very good agreement with the cryo-TEM analysis. At higher q-values, on the other hand, there is an increasing systematic deviation between the data and the fit. As q increases, small vesicles get an increasing weight in the intensity correlation function.[51] One possible reason for the deviation is that the exponential form of $N(R)$ is not expected to be accurate for small radii. In fact we expect very small radii to be energetically strongly unfavorable and a more realistic form of $N(R)$ is rather a function that has a maximum at some radius and then approaches zero for small R. In the analysis above, we have also neglected a time dependence in the vesicle form factor. Vesicles of flexible bilayers are expected to undergo shape fluctuations with an amplitude and frequency dictated by bilayer rigidity.[52,53] Although we expect the amplitudes of these motions to be small and difficult to detect in a polydisperse system we cannot exclude the possibility that they similar to large polymers influence the intensity correlation function since $1 < qR_g^z < 2$, at least for the larger vesicles in the population.[54,55] We postpone a more detailed analysis of DLS data to the future, but conclude here that the DLS data are consistent with the cryo-TEM observation of vesicles having a number-average radius of about 60 nm with a distribution that at least for $R > 50$ nm can be described to a good approximation by an exponential function. When the intensity correlation functions were analyzed by either single-exponential CUMULANT fit or by regularized inverse Laplace transformation,[42] the obtained relaxation rate gave a z-average translational diffusion coefficient, which was q^2-dependent in the lower q range up to $\theta = 34°$. At $q = 0$, the D_z corresponds to the z-average $R_H^z = 192$ nm, which indicates that the intensity size distribution is shifted toward larger sizes compared to $N(R)$, which is centered at 60 nm.

Interestingly, the vesicle size distribution does not seem to vary significantly with the temperature. The increase in scattered intensity that is observed in Figure 2a−e when the temperature is raised could be due to the fact that the number of vesicles is increasing. As shown in Figure 2a−e, the scattered light intensity increases by several orders of magnitude when the temperature is increased from the phase boundary temperature, of approximately 15 °C, up to 25 °C. We believe that the increase in intensity results mainly from an increase in the vesicle concentration, i.e., the vesicle concentration increases while the unimer concentration decreases as the temperature is increased. To further investigate the copolymer self-assembly, NMR self-diffusion and ^{1}H chemical shift experiments were carried out. In pulsed gradient NMR experiments, molecular self-diffusion coefficients can be measured. Experiments were performed both in the L_1 phase and in the $L_1 + L_\alpha$ region, following the echo decay of methyl protons of the PPO block, as described above (Figure 8). Entering the $L_1 + L_\alpha$ region, a slow diffusion mode is introduced in the echo decay, which essentially becomes bimodal. The relative amplitude of the slow mode increases with increasing temperature. Also presented in Figure 8 is the echo decay obtained at 25 °C, where the experiment was optimized to explore a large range of k-values. In the bimodal echo decay, the initial fast mode is similar to the decay observed at 10 °C and arises from copolymers diffusing as unimers. The second, slow, decay corresponds to the diffusion of vesicles. The fact that both modes can be observed separately demonstrates that the two populations do not exchange site during the experimental time scale which at 25 °C was 20 ms. In additional experiments, the experimental time scale was increased up to 1000 ms, still resulting in a bimodal type of decay, this is displayed in Figure 9. We will argue below that the two populations are chemically different, corresponding to different fractions of the polydisperse copolymer material.

The self-diffusion of the vesicles can be analyzed from the slow decay mode. A detailed look at the slow mode revealed

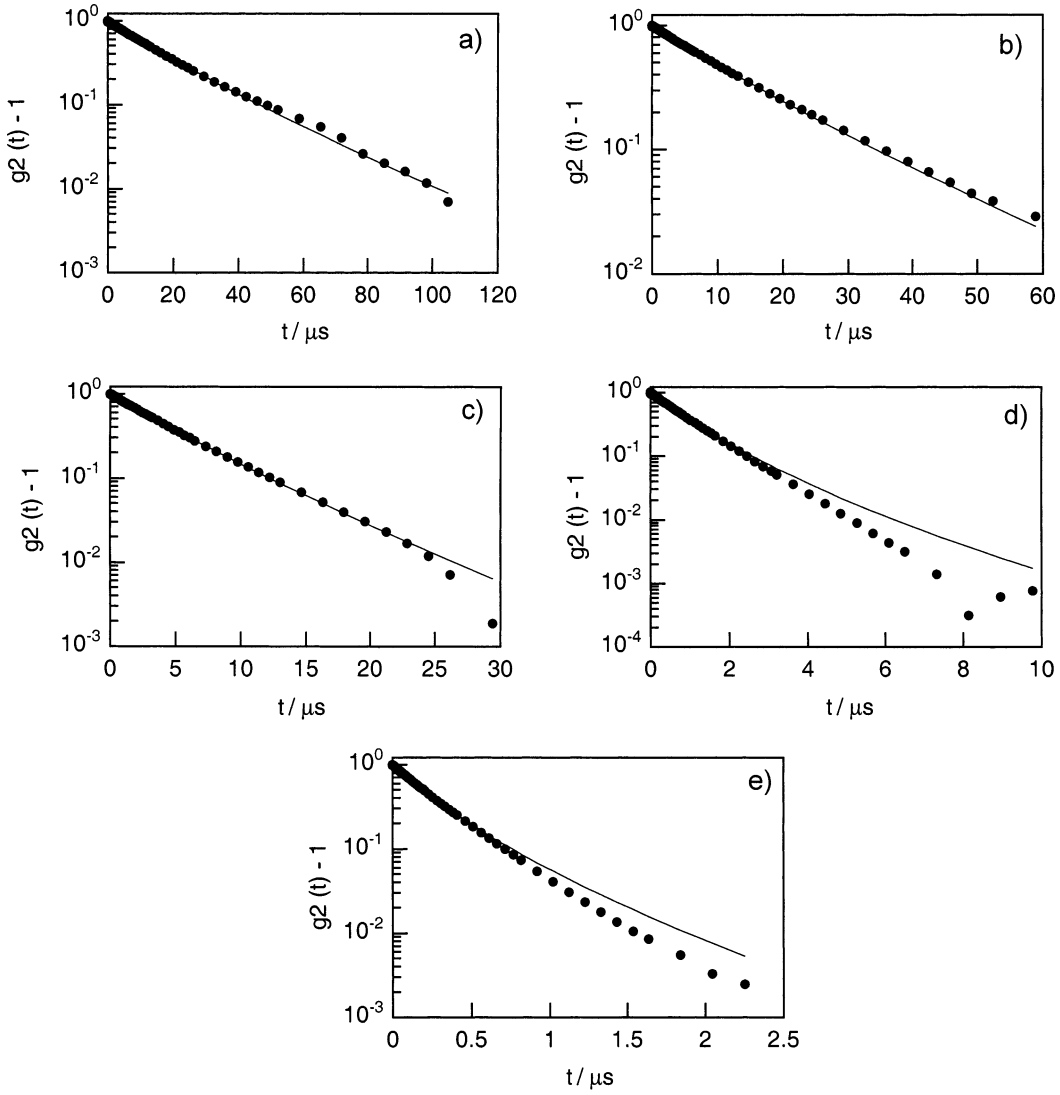

Figure 7. Time−intensity correlation function obtained from the dynamic light scattering measurements for a 0.01 wt % copolymer sample. The solid line represents a least-squares fit of eq 6. (a−e) correspond to measurements at different q-values, 4.65 μm^{-1} ($\theta = 17°$), 5.19 μm^{-1} ($\theta = 19°$), 8.1 μm^{-1} ($\theta = 30°$), 1.57 μm^{-1} ($\theta = 60°$), and 2.57 μm^{-1} ($\theta = 110°$), respectively.

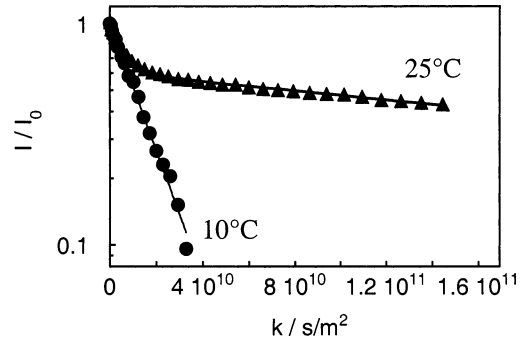

Figure 8. I/I_0 vs k ($k \equiv \gamma^2 g^2 \delta^2 (\Delta - \delta/3)$) for the methyl protons in the PPO block for a 0.01 wt % copolymer sample. The solid line represents a least-squares fit of eq 8 at 25 °C and eq 1 at 10 °C. The parameters at 25 °C were $\delta = 1$ ms, $\Delta = 22.1$ ms, and $g_{max} = 9.63$ T/m; at 10 °C, $\delta = 0.5$ ms, $\Delta = 20$ ms, and $g_{max} = 9.63$ T/m.

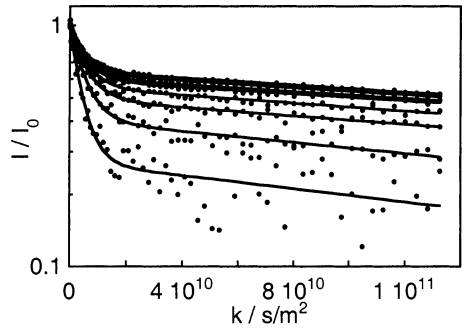

Figure 9. I/I_0 vs k ($k \equiv \gamma^2 g^2 \delta^2 (\Delta - \delta/3) D$) for the methyl protons in the PPO block for a 0.01 wt % copolymer sample. The solid line represents a least-squares fit of eq 8. The attenuation curves are measured at different τ_2; from the top, 18.2 ms, 33.2 ms, 59.3 ms, 105.2 ms, 182.2 ms, 25.3 ms, 570.1 ms, and 998.2 ms.

that this mode is not a pure exponential. In Figure 10, we have plotted separately the slow mode from the 25 °C experiment. Rather, the decay can be described as a sum of exponentials. This implies that also the unimers that have aggregated into vesicles exchange slowly between different vesicles on the experimental time scale so that the polydispersity in the vesicle population is resolved in the echo experiment.

The slow echo decay was fitted by

$$E(k) = \frac{\int_0^\infty R^2 N(R) \exp\{-kD(R)\} dr}{\int_0^\infty R^2 N(R) dr} \qquad (7)$$

with $D(R)$ and $N(R)$, again, given by eqs 3 and 4. The term R^2

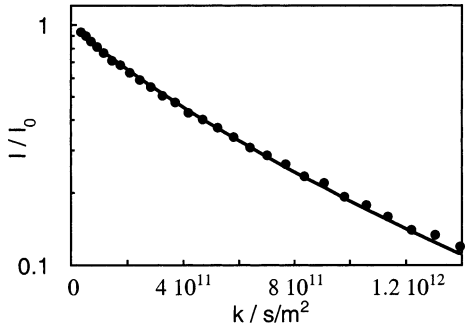

Figure 10. I/I_0 vs k ($k \equiv \gamma^2 g^2 \delta^2 (\Delta - \delta/3) D$) for the methyl protons in the PPO block for a 0.01 wt % copolymer sample. The solid line represents a least-squares fit of eq 7. The parameters were $\delta = 2$ ms, $\Delta = 53.2$ ms, and $g_{max} = 9.63$ T/m.

arises from the fact that the NMR signal is proportional to the number of molecules, which is proportional to the surface area of the vesicle. From the fit, which is shown as a solid line in Figure 10 we obtain the number-average radius $\langle R \rangle = 49$ nm. We conclude that this value is consistent with the DLS data and the cryo-TEM observation. The fact that we obtain a slightly smaller $\langle R \rangle$-value in the echo experiment is probably due to the fact that we have neglected effects of the transverse relaxation time, T_2, in the relative weights of the different vesicle sizes. For the molecules in large vesicles, T_2 is expected to be shorter than that for molecules in small vesicles, hence reducing the relative weight of large vesicles. The self-diffusion coefficient of the unimers at 25 °C was determined to 1.6×10^{-10} m^2 s^{-1} by fitting the data in Figure 8 to a biexponential decay

$$E(k) = I_0 (p_1 \exp(kD_1) + \exp(kD_2)) \qquad (8)$$

where, D_1 and D_2 are the diffusion coefficients and $p_1 + p_2 = 1$. (Note that the slow mode was evaluated from another experiment, Figure 10). This gives a value of the hydrodynamic radius of 1.2 nm and it is smaller than the value 1.9 nm obtained at 10 °C. At 25 °C a significant fraction of the molecules are aggregated into vesicles. The L121 copolymer is polydisperse and, possibly, the vesicles are enriched in high molecular weight components while the unimer fraction is enriched with relatively low molecular weight components, hence the lower hydrodynamic radius of the unimers at 25 °C. Also, as the temperature is increased from 10 to 25 °C, water has become a worse solvent for the PPO as well as the PEO blocks, resulting in less water swollen copolymer coils.

Fraction of Self-Assembled Copolymer. The overall bimodal shape of the echo decay in the NMR diffusion experiment demonstrates that only a fraction of the unimers are aggregated into vesicles and that this fraction increases with increasing temperature. The relative fraction of unimers and aggregated molecules is, however, difficult to determine from the amplitudes of the different diffusion modes, because the relative echo amplitudes also depend on the relaxation times T_1 and T_2.

The chemical shifts of NMR resonances are sensitive to the chemical nature of the surroundings of the spins. Interestingly, the ^{1}H methyl resonances from the PPO block have different chemical shifts in the aggregated and unimer states. This difference is small (0.025 ppm) and could not be resolved at 200 MHz, but was possible to resolve on a 500 MHz instrument. In Figure 11, we show some ^{1}HNMR spectra of the methyl group region recorded at 500 MHz at different temperatures for a copolymer concentration of 0.01 wt %. When increasing the temperature from the L_1 phase and entering the $L_1 + L_\alpha$ region, a second peak appears beside the original resonance of

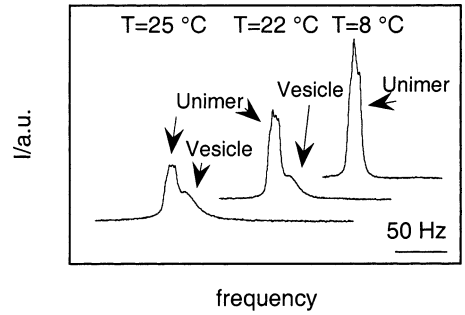

Figure 11. NMR proton spectra of the methyl peak from the polymer at different temperatures, (25 °C, 22 °C, and 8 °C) for a 0.01 wt % copolymer sample. The area under the different parts of the peaks indicated with arrows was determined, and from that the fraction of unimer polymer and vesicle could be estimated.

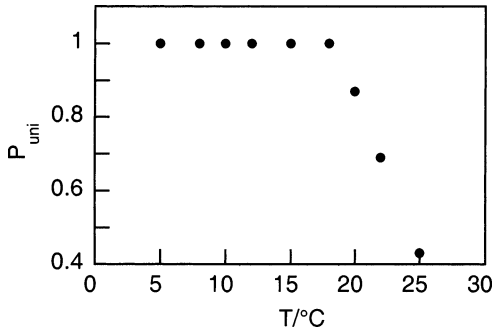

Figure 12. Fraction of unimers as a function of temperature (T) for a 0.01 wt % copolymer sample. The data are obtained from NMR-proton spectra as displayed in Figure 12.

the PPO methyl group in the ^{1}H NMR spectrum. The second signal appearing, which we interpret as corresponding to aggregated molecules, is broader and implies a shorter T_2 that is consistent with the slower dynamics in the aggregated state. The observation of two signals implies a slow molecular exchange between the two states on the time scale of the inverse frequency difference (≈0.08 s). The relative amplitude of the two signals varies with temperature. The broad signal grows at the expense of the original narrow signal with increasing temperature. With the assumption of separate unimer and vesicle signals, we can determine the fraction of aggregated copolymers since the areas under the resonances are proportional to the concentrations of methyl protons in the respective states. The areas under the different signals were determined by fitting a sum of Lorentz functions to the signals and then calculating the relative area under each signal. The results from this analysis are presented in Figure 12 where we have plotted the fraction of unimers, P_{uni}, as a function of temperature. As is seen, P_{uni} decreases with increasing temperature in the $L_1 + L_\alpha$ region. However, at 25 °C, ca. 40% of the copolymer still remains as unimers. Strictly, we have in this way measured the relative concentration of PPO methyl groups in the respective states and not the concentration of unimers. If the unimers have on the average a smaller PPO block, compared to the aggregated ones, which is likely, the P_{uni} values presented in Figure 12 underestimate the molecular fraction of unimers in the $L_1 + L_\alpha$ region. These results are consistent with recent calorimetry (DSC) results on the same system.[49] There the DSC signal reflects the dehydration of the PPO blocks (endothermic process) as the temperature is raised. For this particular system, the DSC scan shows that the aggregation process is not completed at 25 °C, i.e., unimers and vesicles coexist.

Comparing with Mixed Micelles. Self-assembly occurs when passing the phase boundary of the L_1 phase and, as

mentioned above, the temperature-dependent phase boundary concentration, $C^*(T)$, can be viewed as a critical aggregation concentration, similar to the cmc for micelle-forming amphiphiles. The L121 copolymer sample is a mixture of amphiphilic components, *i*, and we expect the first aggregate that forms when we cross the phase boundary to be enriched in the less water-soluble, or hydrophobic, components. If the polydispersity is not too large, we can assume that all components have similar aggregation behavior, i.e., they are not forming micelles but rather form bilayers, with a phase transition to a lamellar phase, as in the mixture, each component having its own phase boundary concentration, $C_i^*(T)$. In this case we can understand the aggregation into vesicles in a way similar to that by which we understand the micellization of mixed amphiphiles.[16] Within the phase separation model we consider the equilibrium between unimers in the bulk and aggregated molecules. Assuming dilute solutions and ideal mixing in the aggregates we have[16]

$$X_i C_i^*(T) = \alpha_i C^*(T) \tag{9}$$

where X_i is the fraction of component *i* in the aggregates, and α_i is its fraction in the overall amphiphilic mixture. The phase boundary of the mixture is then given by

$$C^*(T) = \left(\sum_i \frac{\alpha_i}{C_i^*(T)} \right)^{-1} \tag{10}$$

The first aggregate formed is enriched in the less water-soluble components, having a low phase boundary concentration. The composition of the first aggregate is given by

$$X_i = \alpha_i \frac{C^*(T)}{C_i^*(T)} \tag{11}$$

with $C^*(T)$ given by eq 10, above. With increasing temperature, or total concentration, the composition of the aggregates approaches the overall composition of the mixture. At 25 °C, we found that approximately 40% of the molecules are still in the unimer state, while the overall concentration probably (by extrapolation) is an order of magnitude above C^* at this temperature. This indicates that the relative difference between the lowest and highest C^* in the mixture is at least an order of magnitude at 25 °C. What this means in terms of chemical polydispersity of the Pluronic copolymer is difficult to say. It is known from the literature[56] that by varying the length of the PPO block and keeping the molecular weight constant, the critical micelle concentration (CMC) is decreased by increasing the number of PO segments. The same behavior is observed when the molecular weight is increased but the composition ratio is kept constant; the CMC is decreased when the molecular weight is increased. The effect observed by varying the length of the PEO block is not as pronounced as the effect observed by varying the length of the PPO block. In this last case the CMC is increased when the PEO length is increased. We note, however, that for alkyl chain surfactants, the CMC decreases by approximately 1 order of magnitude when the alkyl chain is enlarged by two CH_2 groups.

Effects of Temperature in the $L_1 + L_\alpha$ Region. We now return to the scattered light intensities recorded as a function of temperature in the $L_1 + L_\alpha$ region and are presented in Figure 2. As is seen in Figure 2, the total scattered intensity, normalized by the incoming laser intensity, increases by approximately 2 orders of magnitude when the temperature is increased from the phase boundary up to room temperature. As discussed above, the vesicle size distribution appears to be very similar at the different temperatures, and we conclude that the strong variation of the scattered intensity is mainly due to the fact that the concentration of vesicles increases with increasing temperature.

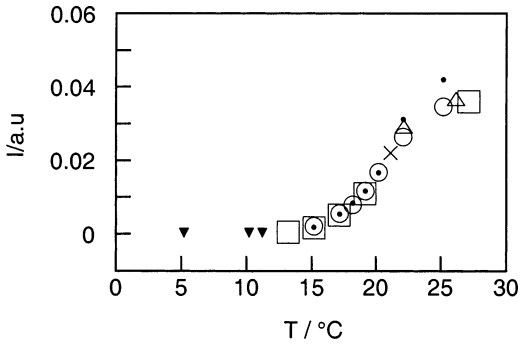

Figure 13. Scattered intensity (*I*) as a function of temperature (*T*) for a 0.01 wt % copolymer sample. The different symbols indicate different experimental series with different temperature cycles. The filled and open symbols represent a decrease or increase of the temperature, respectively. The filled and open circles represent the same sample. (●) = 25 °C to 15 °C, (○) = 15 °C to 25 °C, (□) = 13 °C to 27 °C, (▼) = 5 °C to 11°C, (△) = 22 °C to 26 °C, and (x) = 21 °C.

For a nonequilibrium vesicle dispersion, we would in principle expect the vesicle size distribution to depend on the sample history. In Figure 13, we have replotted the intensity data recorded at $\theta = 90°$ from the 0.01 wt % concentration. Here, the different symbols represent experiments with different temperature histories, i.e., different temperature cycles, and even different prepared samples. In all cases the samples were originally equilibrated in the L_1 phase, at approximately 8 °C. The sample was thereafter placed in the light scattering instrument equilibrated at the chosen starting temperature. The total scattered intensity, normalized by the incoming laser intensity, was recorded after approximately 15 min, and repeated experiments showed that essentially no variation in the intensity could be observed from this time and up to several hours. A new temperature was then chosen by simply changing the temperature of the water-circulating thermostat that controls the temperature of the cell-housing in which the light scattering cell is placed. The time required for equilibrating the new temperature was approximately 15 min, depending on how large a temperature change was made. An additional 15 min waiting time was then used before the intensity was recorded at this temperature. In Figure 13, we see that the scattered intensity at a given temperature is essentially reproduced in the different experiments. This is a striking result. Not only do the data represent experiments on differently prepared samples, the scattered intensity recorded at a given temperature is also essentially independent of the thermal history.

This apparent independence of thermal history can further be illustrated by the experiment presented in Figure 14. Here we have plotted the Rayleigh ratio (total scattered intensity relative to toluene) as a function of the scattering vector, *q*, for a 0.01 wt % L121 solution, measured at two temperatures, 20 and 25 °C, in a temperature cycle. The transmittance (*T*) for a 1 cm path length at 25 °C was determined separately in a UV/Vis spectrophotometer to 0.93, showing that we can neglect any effects of multiple scattering on the recorded scattering curves (since $T > 0.80$).[57] The sample was first equilibrated in the L_1 phase and was then heated to 20 °C. After waiting approximately 120 min at this temperature, the scattering intensity was recorded as a function of *q*. Then, the temperature was increased to 25 °C, where, after a similar waiting time, a

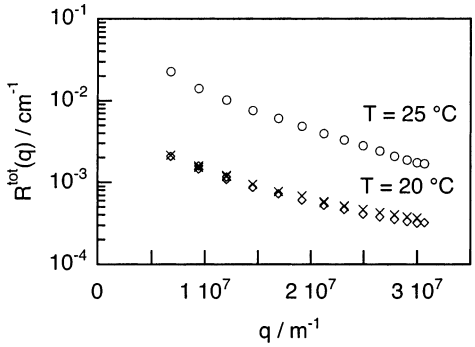

Figure 14. Rayleigh ratio ($R^{tot}(q)$) as a function of the magnitude of the scattering vector (q) for a 0.01 wt % copolymer sample. The data were obtained by first measuring at 20 °C, then at 25 °C, and then lowering the temperature to 20 °C again. The symbols indicate the data from different temperature series. ($\diamond$) = 20 °C (first measurement), ($\circ$) = 25 °C, ($\times$) = 20 °C (second measurement at 20 °C).

second scattering curve was recorded. Finally, the temperature was lowered back to 20 °C where, again after a similar waiting time, the third scattering curve was recorded. As can be seen, the two scattering curves recorded at 20 °C are very similar, indeed, almost identical. This indicates that the vesicle size distribution in the two experiments at 20 °C is very similar, irrespective of the very different temperature histories. In the first case the temperature was approached by heating, while in the second case it was approached by cooling from 25 °C. The scattered intensity varies by approximately an order of magnitude within the measured q-range, which is consistent with the large size of the vesicles. The scattering curves at the two temperatures differ mainly by a proportionality constant, but not exactly. There is a slight difference in the q-dependencies indicating that the vesicle size distribution is not exactly equal at the two temperatures.

Thermodynamic Equilibrium. The fact that the scattering is independent of the thermal history is a striking result. Indeed, the vesicle dispersion essentially behaves as being in thermodynamic equilibrium. Thermodynamic stability of vesicles has been reported previously; however, this is a controversial issue.[58] For bilayers of zero spontaneous curvature, e.g., single component bilayers, vesicles are energetically penalized, but may in principle be stable relative to the lamellar phase due to translational entropy. This is however not generally observed, possibly because it requires concentrations lower than any critical aggregation concentration of the system. With mixed amphiphiles, on the other hand, a spontaneous uneven distribution of the amphiphiles between the inside and outside monolayers may provide a stabilizing mechanism.[59] Considering normal vesicles in water, the basic idea is that if the outside monolayer is preferentially populated by amphiphiles having a spontaneous curvature toward oil, while the inside monolayer is preferentially populated by amphiphiles having a spontaneous curvature toward water. This results in a nonzero spontaneous curvature of the bilayer membrane, stabilizing the curvature of vesicles relative to the planar lamellar morphology. This stabilizing mechanism has also been recognized for block copolymer systems. Focusing on block copolymer polydispersity, Luo and Eisenberg have recently shown using fluorescent labels that, depending on the copolymer composition, there can be different preferences toward the inside or outside monolayers in polystyrene−poly(acrylic acid) vesicles.[31] Possibly, the same mechanism of stabilization is operating in the present system as in the systems studied by Eisenberg et al., and for short times the vesicle dispersion behaves as being in equilibrium and the vesicle concentration can relax when varying the temperature. At long times, however, a sedimentation is observed in the present system. The structure of the sediment has not yet been investigated. The density difference between the copolymer and water is small, and for 50−100 nm vesicles we do not expect a sedimentation of individual vesicles. It may, however, involve aggregated vesicles. An attractive interaction is consistent with the fact that the lamellar phase is not swelling to high water contents. If it is so that the vesicles aggregate, the process is slow, indeed much slower than if it simply would have been diffusion controlled. Another interesting possibility in this system, at least at higher concentrations, is that the high unimer concentration may result in a depletion attraction between vesicles.[60,61] At the low concentrations investigated here, however, these effects are negligible.

4. Summary

We have investigated dilute aqueous solutions of a block copolymer, L121, having the nominal composition $EO_5PO_{68}EO_5$. Below approximately 15 °C the copolymer dissolves as unimers in water (L_1 phase). However, upon heating the system across the phase boundary into the $L_1 + L_\alpha$ two-phase region, above approximately 15 °C, results in vesicle formation. Consistent results from different experimental techniques show that, within the time scale of hours, the vesicle size distribution is essentially independent of the temperature while the concentration of the vesicles increases strongly with the temperature. Furthermore, the size distribution is independent of the thermal history. We conclude that the polydispersity of the copolymer is the main reason for the strong temperature dependence of the vesicle concentration and for a conditional equilibrium of the vesicles due to an uneven distribution of chemically different copolymers between the inside and outside of the vesicles. At longer times, the vesicles are unstable and thermal equilibrium is presumably a concentrated lamellar phase. The mechanistic pathway in the relaxation towards the lamellar phase may involve slow aggregation and/or fusion of vesicles.

Acknowledgment. The authors are grateful to Gunnel Karlsson and Johanna Borne for the cryo-TEM imaging. This work was supported by the Center for Amphiphilic Polymers from Renewable Resources (CAP), Swedish Foundation for Strategic Research (SSF), the former Swedish Natural Science Research Council (NFR), and the Swedish Research Council (VR).

References and Notes

(1) Tuzar, Z.; Kratochvíl, P. In *Surface Colloid Science*; Matijevic', E., Ed.; Plenum Press: New York, 1993; Vol. 15, p 1.

(2) Webber, S. E.; Munk, P.; Tuzar, Z. *Solvents and Self-Organization of Polymers*; Kluwer Academic Publishers: Dordrecht, The Netherlands, 1996.

(3) Alexandridis, P.; Hatton, T. A. *Colloids Surf.* **1995**, *96*, 1.

(4) Alakhov, V. Y.; Kabanov, A. V. *Expert Opin. Invest. Drugs* **1998**, *7*, 1453.

(5) Alexandridis, P. *Curr. Opin. Colloid Interface Sci.* **1996**, *1*, 490.

(6) Edens, M. W. Applications of Polyoxyalkylene Block Copolymer Surfactants. In *Nonionic Surfactants: Polyoxyalkylene Block Copolymers*; Nace, V. M., Ed.; Marcel Dekker Inc: New York, 1996; Vol. 60, p 185.

(7) Chu, B.; Zhou, Z. In *Nonionic Surfactants: Polyoxyalkylene Block Copolymers*; Nace, V. M., Ed.; Marcel Dekker Inc.: New York, 1996; Vol. 60, p 67.

(8) Alexandridis, P. *Curr. Opin. Colloid Interface Sci.* **1997**, *2*, 478.

(9) Nolan, S. L.; Phillips, R. J.; Cotts, P. M.; Dungan, S. R. *J. Colloid Interface Sci.* **1997**, *191*, 391.

(10) Mortensen, K.; Brown, W. *Macromolecules* **1993**, *26*, 4128.

(11) Linse, P. *J. Phys. Chem.* **1993**, *97*, 13896.

(12) Schillén, K.; Brown, W.; Johnsen, R. M. *Macromolecules* **1994**, *27*, 4825.

(13) Schillén, K.; Bryskhe, K.; Mel'nikova, Y. S. *Macromolecules* **1999**, *32*, 6885.

(14) Israelachvili, J. *Intermolecular and Surface Forces*, 2nd ed.; Academic Press: Harcourt & Company, Publishers: New York, 1991.
(15) Lasic, D. D. *Liposomes*; Elsevier: Amsterdam, 1993.
(16) Evans, D. F.; Wennerström, H. *The Colloidal Domain where Physics, Chemistry, Biology and Technology meet*, 2nd ed.; Wiley-VHC: New York, 1998.
(17) Marques, E.; Khan, A.; Miguel, M. d. G.; Lindman, B. *J. Phys. Chem.* **1993**, *97*, 4729.
(18) Joannic, R.; Auvray, L.; Lasic, D. D. *Phys. Rev. Lett.* **1997**, *78*, 3402.
(19) Scleifer, I.; Gerasimov, O. V.; Thompson, D. H. *Proc. Natl. Acad. Sci. U.S.A.* **1998**, *95*, 1032.
(20) Khan, A.; Marques, E. F. *Curr. Opin. Colloid Interface Sci.* **2000**, *4*, 402.
(21) Olsson, U.; Wennerström, H. *J. Phys. Chem. B* **2002**, *106*, 5135.
(22) Zhang, L.; Eisenberg, A. *Science* **1995**, *268*, 1728.
(23) Zhang, L.; Eisenberg, A. *J. Am. Chem. Soc.* **1996**, *118*, 3168.
(24) Ding, J.; Liu, G. *Macromolecules* **1997**, *30*, 655.
(25) Iyama, K.; Nose, T. *Polymer* **1998**, *39*, 651.
(26) Cronelissen, J. J. L. M.; Fischer, M.; Sommerdijk, N. A. J. M.; Nolte, R. J. M. *Science* **1998**, *280*, 1427.
(27) Holder, S. J.; Hiorns, R. C.; Sommerdijk, N. A. J. M.; Williams, S. J.; Jones, R. G.; Nolte, R. J. M. *Chem. Commun.* **1998**, 1445.
(28) Kukula, H.; Schlaad, H.; Antonietti, M.; Förster, S. *J. Am. Chem. Soc.* **2002**, *124*, 1658.
(29) Harris, J. K.; Rose, G. D.; Bruening, M. L. *Langmuir* **2002**, *18*, 5337.
(30) Zhang, L.; Eisenberg, A. *Polym. Adv. Technol.* **1998**, *9*, 677.
(31) Luo, L.; Eisenberg, A. *J. Am. Chem. Soc.* **2001**, *123*, 1012.
(32) Yu, Y.; Zhang, L.; Eisenberg, A. *Langmuir* **1997**, *13*, 2578.
(33) Kinning, D. J.; Winey, K. I.; Thomas, E. L. *Macromolecules* **1988**, *21*, 3502.
(34) Koizumi, S.; Hasegawa, H.; Hashimoto, T. *Makromol. Chem., Macromol. Symp.* **1992**, *62*, 75.
(35) Siqueira, D. F.; Nunes, S. P. *Polymer* **1994**, *35*, 490.
(36) Laurer, J. H.; Fung, J. C.; Sedat, J. W.; Smith, S. D.; Samseth, J.; Mortensen, K.; Agard, D. A.; Spontak, R. J. *Langmuir* **1997**, *13*, 2177.
(37) Zipfel, J.; Lindner, P.; Tsianou, M.; Alexandridis, P.; Richtering, W. *Langmuir* **1999**, *15*, 2599.
(38) Bryskhe, K.; Schillén, K.; Löfroth, J.-E.; Olsson, U. *Phys. Chem. Chem. Phys.* **2001**, *3*, 1303.
(39) Brown, W.; Schillén, K.; Almgren, M.; Hvidt, S.; Bahadur, P. *J. Phys. Chem. B* **1991**, *95*, 1850.
(40) Brown, W.; Schillén, K.; Hvidt, S. *J. Phys. Chem. B* **1992**, *96*, 6038.
(41) Schillén, K.; Claesson, P. M.; Malmsten, M.; Linse, P.; Booth, C. *J. Phys. Chem. B* **1997**, *101*, 4238.
(42) Jansson, J.; Schillén, K.; Olofsson, G.; da Silva, R. C. *J. Phys. Chem. B* **2004**, *108*, 82.
(43) Linse, P. *Macromolecules* **1994**, *27*, 2685.
(44) Linse, P. *Macromolecules* **1994**, *27*, 6404.
(45) Bellare, J. R.; Davis, H. T.; Scriven, L. E.; Talmon, Y. *J. Electron Microsc. Technique* **1988**, *10*, 87.
(46) Tanner, J. E. *J. Chem. Phys.* **1970**, *52*, 2523.
(47) Nilsson, P.-G.; Wennerström, H.; Lindman, B. *Chemica Scripta* **1985**, *25*, 67.
(48) Lindman, B.; Wennerström, H. *J. Chem. Phys.* **1991**, *95*, 6053.
(49) da Silva, R. C.; Olofsson, G.; Schillén, K.; Loh, W. *J. Phys. Chem.* **2002**, *106*, 1239.
(50) Pencer, J.; White, G. F.; Hallett, F. R. *Biophys. J.* **2001**, *81*, 2716.
(51) Pusey, P. N.; Megan, W. v. *J. Chem. Phys.* **1984**, *80*, 3513.
(52) Millner, S. T.; Safran, S. A. *Phys. Rev. A* **1987**, *36*, 4371.
(53) Brocca, P.; Cantù, L.; Corti, M.; Favero, E. D. *Prog. Colloid Polym. Sci.* **2000**, *115*, 181.
(54) Burchard, W. In *Light Scattering Principles and Development*, 1st ed.; Brown, W., Ed.; Oxford University Press: Oxford, 1996.
(55) Berne, B. J.; Pecora, R. *Dynamic Light Scattering with Applications to Chemistry, Biology and Physics*, 2nd ed.; Dover Publications Inc.: New York, 2000; Vol. 1.
(56) Alexandridis, P.; Hatton, A. T. *Colloids Surfaces A* **1995**, *96*, 1.
(57) Cotton, J. P. In *Neutron, X-ray and Light Scattering: Introduction to an Invetigative Tool for Colloidal and Polymeric Systems*; Lindner, P., Zemb, T., Eds.; North-Holland: Amsterdam, 1991; p 19.
(58) Laughlin, R. G. *Colloids Surf. A* **1997**, *128*, 27.
(59) Safran, S. A.; Pincus, P.; Andelman, D. *Science* **1990**, *248*, 354.
(60) Asakura, S.; Oosawa, F. *J. Chem. Phys.* **1954**, *22*, 1255.
(61) Vrij, A. *Pure Appl. Chem.* **1976**, *48*, 471.